ImmunoHorizons

RESEARCH ARTICLE

Innate Immunity

Bruton Tyrosine Kinase Inhibition Decreases Inflammation and Differentially Impacts Phagocytosis and Cellular Metabolism in Mouse- and Human-derived Myeloid Cells

Rochelle Y. Benoit, Jennifer L. Zagrodnik, Samantha J. Carew, and Craig S. Moore

Division of Biomedical Sciences, Faculty of Medicine, Memorial University of Newfoundland, St. John's, Newfoundland and Labrador, Canada

ABSTRACT

Bruton tyrosine kinase (BTK) is a kinase expressed by various immune cells and is often activated under proinflammatory states. Although the majority of BTK-related research has historically focused on B cells, understanding the role of BTK in non-B cell populations is critical given myeloid cells also express BTK at comparable levels. In this study, we investigated and compared how BTK inhibition in human and murine myeloid cells alters cell phenotype and function. All experiments were performed using two BTK inhibitors (evobrutinib and tolebrutinib) that are currently in late-stage clinical trials for the treatment of multiple sclerosis. Assays were performed to assess the impact of BTK inhibition on cytokine and microRNA expression, phagocytic capacity, and cellular metabolism. In all cells, both evobrutinib and tolebrutinib significantly decreased phosphorylated BTK and LPS-induced cytokine release. BTK inhibition also significantly decreased the oxygen consumption rate and extracellular acidification rate in myeloid cells, and significantly decreased phagocytosis in murine-derived cells, but not human macrophages. To further elucidate the mechanism, we also investigated the expression of microRNAs known to impact the function of myeloid cells. BTK inhibition resulted in an altered microRNA expression profile (i.e., decreased miR-155-5p and increased miR-223-3p), which is consistent with a decreased proinflammatory myeloid cell phenotype. In summary, these results provide further insights into the mechanism of action of BTK inhibitors in the context of immune-related diseases, while also highlighting important species-specific and cell-specific differences that should be considered when interpreting and comparing results between preclinical and human studies. *ImmunoHorizons*, 2024, 8: 652–667.

INTRODUCTION

Bruton tyrosine kinase (BTK) is a nonreceptor tec kinase within the cytoplasm of hematopoietic cells and contains a kinase domain that possesses various tyrosine residues that can be phosphorylated and result in enzyme activation (1, 2). After cell activation via pattern recognition receptors, BCRs, TLRs, Fc receptors, and/or chemokine receptors, BTK is phosphorylated at its Y-551 residue, which leads to subsequent autophosphorylation of its Y-223 residue (3–8). Once activated, phosphorylated BTK (p-BTK) can activate the NF-κB, NFAT, and/or ERK1/2 signaling pathways, and increase proinflammatory cytokine expression, including IL-1β, IL-6, IL-18, and TNF (9–12).

Within lymphocytes, BTK is predominantly expressed in B cells with minimal expression in T cells and plasma cells (13). In 1952, BTK was first discovered by Ogden Bruton while treating a patient who lacked serum IgG and had recurrent pneumonia; this condition was subsequently named X-linked agammaglobulinemia (XLA), or Bruton's syndrome (14). More recently, BTK has been extensively studied in the context of

Received for publication August 7, 2024. Accepted for publication August 13, 2024.

Address correspondence and reprint requests to: Dr. Craig S. Moore, Memorial University of Newfoundland, 300 Prince Philip Drive, St. John's, NL A1B 3V6, Canada. E-mail address: craig.moore@mun.ca

ORCIDs: 0000-0002-5691-9871 (S.J.C.); 0000-0003-3333-435X (C.S.M.).

Abbreviations used in this article: A/A, antibiotic/antimycotics; BBB, blood-brain barrier; BMDM, bone marrow–derived macrophage; BTK, Bruton tyrosine kinase; BTKi, BTK inhibitor; CLL, chronic lymphoid leukemia; ECAR, extracellular acidification rate; ICC, immunocytochemistry; MCL, mantle cell leukemia; MDM, monocyte-derived macrophage; MS, multiple sclerosis; OCR, oxygen consumption rate; p-BTK, phosphorylated BTK; XLA, X-linked agammaglobulinemia.

https://doi.org/10.4049/immunohorizons.2400045

ImmunoHorizons is published by The American Association of Immunologists, Inc.

several B cell malignancies, including chronic lymphoid leukemia (CLL) and mantle cell leukemia (MCL) (15–17). Using both covalent and noncovalent small-molecule BTK inhibitors (BTKis) that target the C-terminal kinase domain, phosphorylation of the kinase can be inhibited, which prevents B cell development and IgG production, and results in favorable clinical outcomes for patients (18). In 2014, ibrutinib became one of the first Food and Drug Administration (FDA)–approved BTKis for the treatment of CLL, MCL, and other B cell malignancies. Within tumor microenvironments, BTKis have also been investigated for their ability to influence myeloid cell activity by targeting myeloid-derived suppressor cells and tumor-associated macrophages, while also enhancing their ability to respond to microbial and viral infections (19–21). In autoimmune conditions, both the innate and the adaptive immune systems contribute to chronic inflammation and loss of function. Because B cells play a significant role in contributing to the pathophysiology of most autoimmune conditions, BTKis have been investigated for treating several diseases (e.g., rheumatoid arthritis, systemic lupus erythematosus, Sjögren's disease, psoriasis, multiple sclerosis [MS]) and have yielded promising results (22).

Beyond the B cell, myeloid-lineage cells (i.e., macrophages, monocytes, neutrophils, and organ-resident macrophages) express BTK at comparable levels; thus, targeting BTK activity within myeloid cells has been suggested to also contribute to the overall mechanism of action for several BTKis (23–25). To demonstrate a clear importance of studying BTK inhibition outside the context of B cells, previous experiments were performed that selectively transfected *btk*$^{-/-}$ mice infected with *Streptococcus pneumoniae* with *btk* in either B cells alone or in both B cells and myeloid cells. Interestingly, B cell–specific expression of *btk* did not protect mice against infection. In contrast, mice had a significant defense response against bacterial infection when *btk* was expressed in B cells, dendritic cells, and macrophages (25). In models of neuroinflammation and immune-mediated demyelination, BTK inhibition can also modulate both B cell and microglia and result in favorable outcomes (11, 26–29). Specifically, a recent study assessing the effects of BTKis in an animal model of MS demonstrated that after 4 wk of evobrutinib treatment, mice had a 30% reduction in immune cells within the area of meningeal inflammation compared with controls (24). Evobrutinib also reduced the proinflammatory activation of microglia in both a chronic and an adoptive transfer model of experimental autoimmune encephalomyelitis, while also promoting clearance of myelin debris within microglia that increased the rate of remyelination (30).

The objective of this study was to investigate and expand the known mechanism(s) of action of BTKis in myeloid cells. In our experiments, two different BTKis (evobrutinib and tolebrutinib) were compared. To investigate any species-specific effects of BTK inhibition in myeloid cells, we also made comparisons between both primary human- and murine-derived myeloid cells. To assess how BTK inhibition can influence overall myeloid cell function, we used a variety of assays to measure cytokine and microRNA expression, phagocytic capacity, and cellular metabolism.

MATERIALS AND METHODS

Whole blood assays

All studies involving human samples received institutional review board approval at Memorial University of Newfoundland (Health Research Ethics Authority) and strictly followed Canadian Institute of Health Research guidelines. Human whole blood was drawn by a trained phlebotomist and placed in EDTA purple cap 10-ml tubes (366643; BD Canada). Whole blood was diluted 1:5 in RPMI-1640 (31800-022; ThermoFisher) in 5-ml round-bottom polystyrene tubes (352235; Falcon) and was used at a working volume of 500 μl. Whole blood was incubated at 37°C in 5% CO_2.

Human monocyte-derived macrophages

Whole blood (20 ml) was collected in two 10-ml EDTA purple cap tubes (366643; BD Canada). Whole blood serum and PBMC separation were performed by adding 20 ml of whole blood to a 50-ml SepMate tube (85450; STEMCELL Technologies) on top of 15 ml of Ficoll (17144003; Cytiva). The remainder volume of the SepMate tube was filled with PBS. SepMate tubes were spun at 1200 × *g* with the brake on for 10 min to separate out RBCs and granulocytes. The top layer (∼35 ml) of the SepMate tube containing PBMCs was poured into a 50-ml Falcon tube (352070; Falcon). This volume was topped to 50 ml with PBS and centrifuged at 300 × *g* for 15 min with the brake on to pellet the PBMCs. The pellet was then resuspended in 20 ml of MACS buffer (PBS + EDTA [0.002M]; BP118; ThermoFisher) plus FBS (0.5%; FB12999102; Fisher), washed with an additional 30 ml of PBS, and centrifuged at 300 × *g* for 10 min to pellet PBMCs. The PBMC pellet was resuspended in 80 μl of MACS buffer and 20 μl of anti-CD14$^+$ MicroBeads (130-050-201; Miltenyi Biotec) per 1×10^7 cells. The suspension was incubated at 4°C for 15 min. After incubation, 20 ml of MACS buffer was added, cells were centrifuged at 300 × *g* for 10 min, and the cell pellet was then resuspended in 1 ml of MACS buffer. Large magnetic columns (130-042-401; Miltenyi Biotec) were prepared by first adding 3 ml of MACS buffer to prime the column. The columns were then attached to a magnet separator (130-091-051; Miltenyi Biotec), and the cell suspension was applied and allowed to flow through the columns. After 3 × 3 ml washes using MACS buffer, the column containing the CD14$^+$ cells was removed from the magnet separator and placed on a 15-ml tube (352196; Fisher). A total of 5 ml of MACS buffer was applied to the column and pushed through using a syringe plunger to collect all CD14$^+$ cells. MACS buffer (10 ml) was added to the tube and centrifuged at 300 × *g* for 10 min. CD14$^+$ cells were resuspended, counted, and plated at a concentration of 5×10^5 cells/ml in tissue culture–treated dishes. Cells were differentiated into macrophages in RPMI-1640 supplemented with FBS (10%) (FB12999102; Fisher), antibiotic/antimycotics (A/A; 15240-062; Life Technologies), GlutaMAX (35050-061; Life Technologies), and M-CSF (25 ng/ml; 300-25; PeproTech). At 48 h, a 50% media change + 100% M-CSF replenish was performed.

https://doi.org/10.4049/immunohorizons.2400045

Cells were incubated at 37°C in 5% CO_2 and used for all assays on day 5.

Mouse bone marrow–derived macrophages

All animal experiments were approved by the Memorial University Animal Care Committee in accordance with the Canadian Council on Animal Care guidelines. Adult mice were euthanized with CO_2 asphyxiation followed by cervical dislocation. Mice were cleaned with 70% ethanol to disinfect, a cut was made over the peritoneum, and skin was pulled downward to expose the hind limbs. Hind limbs were removed by cutting at the hip, and muscle tissue was removed to expose the femurs, tibias, and fibulas. Bones were submerged in ice-cold PBS (one mouse/tube). Bones were transferred to a petri dish containing ice-cold PBS, and the ends of the bones were removed to expose the bone marrow. In a separate petri dish, bones were flushed with 1 ml of ice-cold PBS and was repeated with the same 1 ml of PBS until all bones were flushed. The 1 ml was transferred to a 15-ml Falcon tube (352196; Fisher) and triturated to remove any clumps. Ice-cold ammonium chloride solution (3 ml; 07850; STEMCELL Technologies) was added to the tubes and incubated on ice for 10 min to lyse all RBCs. PBS (10 ml) was then added, and cells were centrifuged at 300 × *g* for 10 min. The cell pellet was resuspended in complete DMEM (12100-046; ThermoFisher) and plated in nonadherent 10-cm dishes (three dishes/mouse). Cells were differentiated to BMDMs in DMEM (12100-046; ThermoFisher) supplemented with FBS (10%) (FB12999102; Fisher), A/A (15240-062; Life Technologies), GlutaMAX (35050-061; Life Technologies), and M-CSF (10 ng/ml, 300-25; PeproTech). On day 3, 5 ml of additional macrophage media was added to all dishes. On day 7, cells were removed from the dishes using a cell scraper (08-100-240; Fisher) and counted. Cells were then plated at 2.5×10^5 cells/ml, incubated at 37°C in 5% CO_2, and used for assays within 1–2 d.

Mixed glia and microglia

Mixed glia cultures were used to obtain a pure microglia culture. Initial preparations of a papain digestion enzyme mix (1.95 ml/2 mice) and DNase solution (30 μl/2 mice) were prepared from the neural dissection kit (130-092-628; Miltenyi Biotec); the digestion enzyme was placed in gentleMACS C Tubes (130-096-334; Miltenyi Biotec) at 37°C. DNase solution was stored on ice. Cell culture media were prepared (DMEM supplemented with FBS [10%] [FB12999102; Fisher], A/A [15240-062; Life Technologies], and GlutaMAX [35050-061; Life Technologies]) and pre-incubated at 37°C. Six-centimeter dishes were placed on ice blocks, 1 ml of $HBSS^{-/-}$ (Thermo Fisher, Mississauga, ON, Canada) was added (one dish per two brains), and 1 ml of $HBSS^{-/-}$ (14175095; Thermo Fisher) was added to a 1.5-ml Eppendorf and kept on ice (one tube/two mice). One additional 10-cm dish was filled with 10 ml of $HBSS^{-/-}$ (14175095; Thermo Fisher) and placed on ice. Mouse pups (postnatal 0–4 d) were decapitated, brains removed, and placed into the 6-cm dish. The cortices and hippocampi were dissected, and all meninges were removed using tweezers. The two sets of cortices and hippocampi were transferred into the 1.5-ml tube (repeated for total number of brains). The previously prepared DNase solution was added to the papain digestion enzyme (130-092-628; Miltenyi Biotec) in the gentleMACS C tubes (130-096-334; Miltenyi Biotec). The brain tissue from two pups was added to a gentleMACS C tube (130-096-334; Miltenyi Biotec) and gently triturated. Tissue dissociation was performed using the gentleMACS dissociator (130-093-235; Miltenyi Biotec) as per the manufacturer's guidelines. $HBSS^{+/+}$ (2 ml; ThermoFisher, 14025092) was then added to the cell suspension, placed through a 70-μm strainer, and two washes of 5 ml of $HBSS^{+/+}$ (14025092; ThermoFisher) were applied to the filter. Cells were then centrifuged at 300 × *g* for 10 min with the brake on. The cell pellet was resuspended with DMEM (12100-046; ThermoFisher) supplemented with FBS (10%) (FB12999102; Fisher), A/A (15240-062; Life Technologies), and GlutaMAX (35050-061; Life Technologies), and cells were cultured in a T-75 flask. A 50% media change was performed once a week to feed the cells. Once confluent and after 2–3 wk, the flasks were shaken (250 rpm for 3 h) to obtain floating microglia. Microglia were plated at 2.5×10^5 cells/ml in astrocyte conditioned media and incubated at 37°C in 5% CO_2. Astrocyte conditioned media consisted of serum-free DMEM (12100-046; Fisher), supplemented with A/A (15240-062; Life Technologies) and GlutaMAX (35050-061; Life Technologies) that was used to culture mixed glia for 3 d.

BTKi treatments

Human whole blood, monocyte-derived macrophages (MDMs), bone marrow–derived macrophages (BMDMs), and microglia were pretreated with either tolebrutinib (HY-109192; MedChemExpress) or evobrutinib (S8777; Selleckchem) at a dose range of 0.1–10 μM for 24 or 48 h in complete media containing 1% FBS. DMSO was used as a vehicle control. Cells were then ready for use in downstream assays.

Immunocytochemistry and quantification

MDMs, BMDMs, and microglia were plated on four- or eight-well uncoated glass chamber slides (154534PK; Thermo Scientific). After 2–3 d, cells were treated with tolebrutinib or evobrutinib as mentioned earlier. LPS (100 ng/ml; 297-472-0; Sigma) was added to the cells for 30 min. Media were then suctioned off and replaced with a 4% paraformaldehyde solution (MKCS9056; Sigma) for 5 min and then replaced with PBS. Chambers were removed and cells were blocked with normal goat serum (5%) (31872; ThermoFisher) in PBS-Triton X (0.3%) (T8787; Sigma) for 1 h. A primary Ab (p-BTK [Rb] at 1:200; NBP-78295ss; NovusBio) was added to PBS-T and incubated overnight at 4°C. Slides were then washed with PBS (5 ml × 3), and a secondary goat anti-rabbit Ab (AF647, 1:500; A11012; Life Technologies) was added for 2 h at room temperature. Slides were again washed with PBS (5 ml × 3), and DAPI (D1306; Life Technologies) was added at a 1:10,000 dilution in PBS and incubated for 10 min at room temperature before coverslipping

using Fluoromount-G mounting media (0100-01; Southern Biotech). Slides were nail polished and stored at 4°C. All images were acquired on a Zeiss Observer.Z1 microscope. Image quantification for relative fluorescence was performed using ImageJ. Tiff images were converted to 8-bit. The watershed process was applied to separate nuclei in proximity. Outlines were laid around the nuclei and analyzed to obtain a total cell count. Cell bodies were analyzed for fluorescence intensity by selecting integrated density, which provided raw integrated density value/cell count to quantify brightness intensity between treatment conditions. N denotes number of biological replicates; n denotes number of images taken per treatment for each biological replicate.

ELISA

Cell culture supernatants were collected and stored at −80°C. Supernatants were assayed for TNF, IL-6, and IL-10 using an ELISA (555212, 558534, 555220, 555240, 555157, 555252; BD Biosciences) and performed according to the manufacturer's instructions. Cell protein was also collected and assayed for p-BTK using an ELISA (23843; Cell Signaling) as per manufacturer's instructions.

Seahorse assay

MDMs, BMDMs, and microglia were seeded at 100,000 cells/well in 24-well Seahorse plates following the same plating protocol as earlier. Cells were pretreated with tolebrutinib or evobrutinib as mentioned earlier, and LPS (100 ng/ml) was added overnight and incubated at 37°C with 5% CO_2. Cells were then subjected to the Mito Stress Test Kit (103015-100; Agilent Technologies, Mississauga, ON, Canada) using the metabolic inhibitors oligomycin, FCCP, and rotenone/antimycinA as per manufacturer's instructions. Oxygen consumption rate (OCR) and extracellular acidification rate (ECAR) representing oxidating phosphorylation and glycolysis, respectively, were measured using the Seahorse XFe24 analyzer (Agilent Technologies). Data were exported to Microsoft Excel for analysis. OCR (pmol/min) and ECAR (mpH/min) were analyzed separately and graphed to demonstrate any respiratory changes.

Live-cell phagocytosis assay

MDMs, BMDMs, and microglia were seeded in 96-well plates in phenol red–free DMEM or RPMI-1640 (31053028, 11835030; ThermoFisher) supplemented with A/A (15240-062; Life Technologies) and GlutaMAX (35050-061; Life Technologies) following the same protocol as earlier. pHrodo Red Zymosan BioParticles (A10025; 0.125 mg/ml; ThermoFisher) were added to all wells except for control wells. Cells were incubated at 37°C with 5% CO_2 in a live-imaging plate reader (Cytation5), and fluorescence intensity was measured at 5-min intervals over a period of 6 h. Raw data were displayed as fluorescence intensity measurements at 555 nm excitation and 585 nm emission from 0 to 6 h. Data were exported and graphed in an *xy* table format, where fluorescence was shown on the *y*-axis as it changed over time shown on the *x*-axis. All data were normalized to the control group (LPS + pHrodo Red; Zymosan BioParticles).

RNA extraction and quantitative PCR

Cells were lysed in QIAzol reagent (79306; Qiagen) and stored at −80°C until use. RNA was subsequently purified with the RNeasy Micro Kit with DNase treatment (74104; Qiagen). The NanoDrop (ThermoFisher) was used to quantify RNA values. RNA was diluted to 10 ng/μl for reverse transcription using M-MLV reverse transcriptase kit (28025-021; ThermoFisher). In brief, RNA samples were added to a combination of dNTP, RT enzyme, RT buffer, RNase inhibitors, and RNase-free water (28025-021; ThermoFisher) in conjunction with TaqMan probes for miRNA miR-223-3p (002295; ThermoFisher), miR-155-5p (002623; ThermoFisher), miR-21-5p (000397; ThermoFisher), RNU48 (human; 001006; ThermoFisher), and Sno202 (mouse; 001232; ThermoFisher). Mixed samples were subsequently heated in a preprogrammed thermocycler and prepared cDNA was stored at −20°C until use. Reverse-transcriptase quantitative PCR (RT-qPCR) was carried out using TaqMan Fast Universal PCR Master mix (4444557; Applied Biosystems) and microRNA-specific TaqMan primers as follows: miR-223-3p (002295; ThermoFisher), miR-155-5p (002623; ThermoFisher), miR-21-5p (000397; ThermoFisher), RNU48 (human; 001006; ThermoFisher), and Sno202 (mouse; 001232; ThermoFisher). miRNA expression was normalized to a combination of RNU48 (human) and Sno202 (mouse) reference miRNA. Fold changes were calculated using the ΔΔCT method.

Statistical analysis

All data analysis was done using GraphPad Prism (Version 10). For immunocytochemistry (ICC) and ELISA quantification, a one-way ANOVA was used, and data were presented as the mean ± SEM. Multiple comparison tests were done, and all group comparisons were finalized to compare with the control group (LPS + DMSO). Cytokine ELISAs were normalized to percent maximum (DMSO + LPS) to account for variation between individual human/animal cells.

RESULTS

Evobrutinib and tolebrutinib significantly decrease phosphorylation of BTK in human and mouse myeloid cells

ICC was used to measure the ability of evobrutinib and tolebrutinib to decrease the phosphorylation of BTK under LPS-stimulated conditions. Images of human MDMs, mouse BMDMs, and mouse microglia were acquired to determine whether the inhibitors decreased p-BTK (Fig. 1A–C). Image quantification of the p-BTK signal was performed using ImageJ to identify differences in fluorescence intensity across conditions. In the presence of LPS, MDMs had a significant decrease in fluorescence intensity in the presence of a BTKi (1 μM evobrutinib and tolebrutinib; Fig. 1D). A wide dose range was initially performed (0.1 nM to 10 μM) to determine a dose–response curve

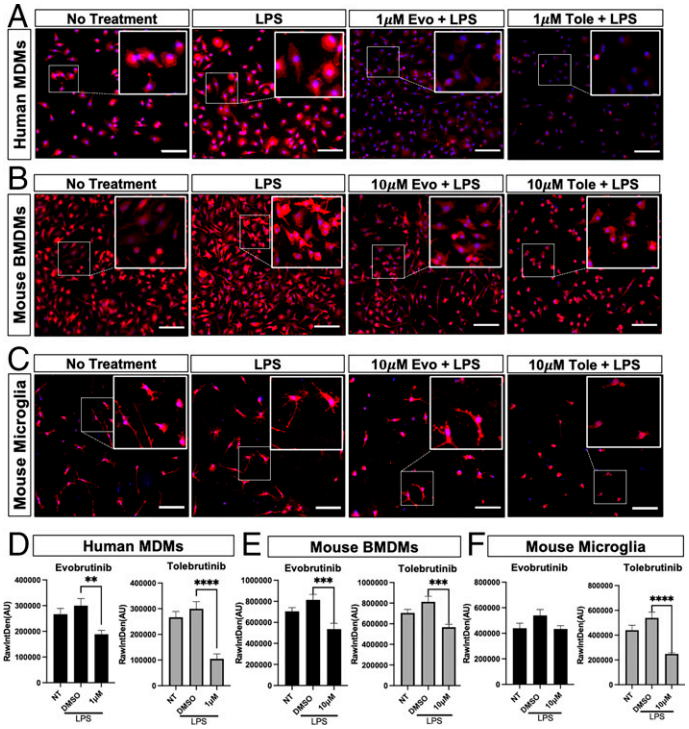

FIGURE 1. BTKis tolebrutinib and evobrutinib significantly decrease phosphorylation of BTK in human and mouse myeloid cells.
(**A**–**C**) ICC images of p-BTK (red) and DAPI (blue) in human MDMs, mouse BMDMs, and microglia (scale bars, 100 μm). (**D**–**F**) A significant decrease in p-BTK is shown in (D) MDMs, (E) BMDMs, and (F) microglia through quantification of ICC images in (A)–(C) ($N = 3$, $n = 6$ per treatment per cell type). DMSO: 0.1%, 10 μM. Statistical analysis was performed using a one-way ANOVA with the main comparator group being DMSO + LPS. $^{**}p < 0.01$, $^{***}p < 0.001$, $^{****}p < 0.0001$. Error bars represent mean ± SEM. AU, arbitrary units; NT, no treatment.

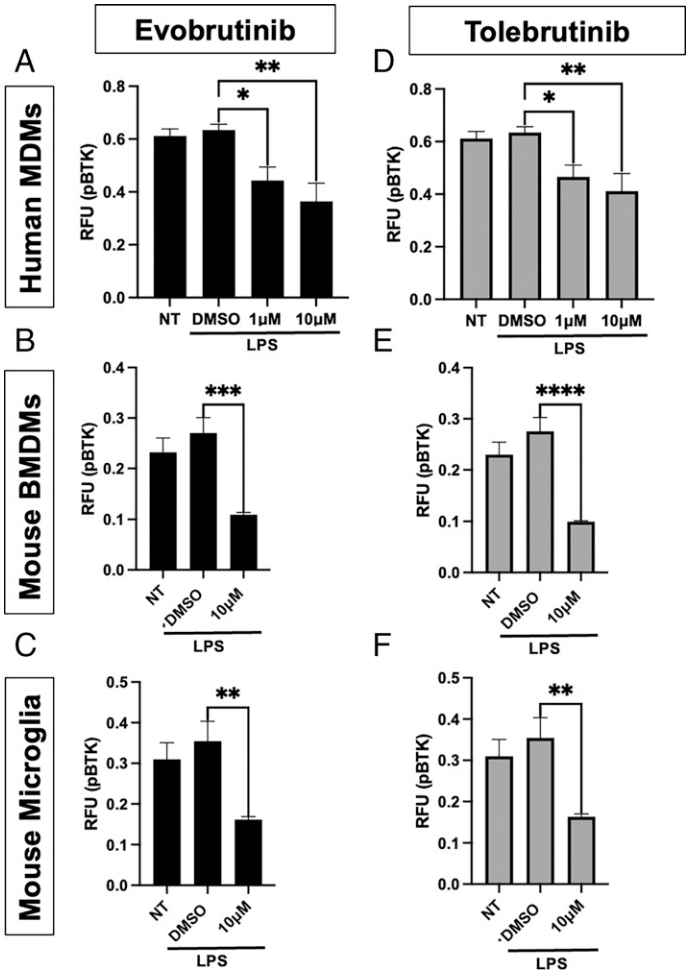

FIGURE 2. BTKis tolebrutinib and evobrutinib significantly decrease p-BTK protein expression in human and mouse myeloid cells.
(**A**–**C**) Evobrutinib significantly decreased p-BTK levels in (A) human MDMs, (B) mouse BMDMs, and (C) microglia. (**D**–**F**) Tolebrutinib significantly decreased p-BTK levels in (D) MDMs, (E) BMDMs, and (F) microglia ($n = 6$ per treatment per cell type). DMSO: 0.1% at 10 μM. Statistical analysis was performed using a one-way ANOVA with the main comparator group being DMSO + LPS. $^{*}p < 0.05$, $^{**}p < 0.01$, $^{***}p < 0.001$, $^{****}p < 0.0001$. Error bars represent mean ± SEM. NT, no treatment; RFU, relative fluorescence units.

and optimal concentration that resulted in a significant decrease in p-BTK. To prevent any potential off-target effects, we used the lowest dose of the BTKi where a trough effect was observed (1 μM in human-derived cells and 10 μM in mouse-derived cells). In all subsequent experiments, the dose of the specific BTKi was selected based on their pharmacodynamics and ability to inhibit p-BTK. Furthermore, using a propidium iodide uptake assay, doses of the BTKis within this range did not result in cell death (data not shown). Mouse cells responded similarly, whereby both evobrutinib and tolebrutinib (10 μM) significantly decreased p-BTK in BMDMs (Fig. 1E); in mouse microglia, tolebrutinib (10 μM) also significantly decreased p-BTK (Fig. 1F). To confirm the ICC results, we also used an ELISA to quantify p-BTK within protein lysates. Similar to the ICC results, using a p-BTK ELISA, both evobrutinib and tolebrutinib significantly decreased p-BTK levels in human MDMs, mouse BMDMs, and primary mouse microglia (Fig. 2); levels of BTK remained unchanged (via ELISA and Western blot) upon BTKi treatment, whereas normalization of p-BTK to total BTK levels gave similar results (data not shown) (Figs. 1, 2).

Evobrutinib and tolebrutinib decrease cytokine production in human and mouse myeloid cells

Under similar activation conditions as earlier, an ELISA was used to measure cytokine levels (TNF, IL-6, and IL-10) within the cell supernatants to assess the downstream effects of inhibiting BTK in myeloid cells under inflammatory conditions. In human whole blood, both evobrutinib and tolebrutinib dose-dependently decreased TNF levels; decreased IL-6 production was also observed (Fig. 3A). In human MDMs, both evobrutinib and tolebrutinib significantly decreased TNF and IL-10; no effect was observed on IL-6 (Fig. 3B). To investigate possible species differences (human versus mouse) upon BTKi treatment, we also

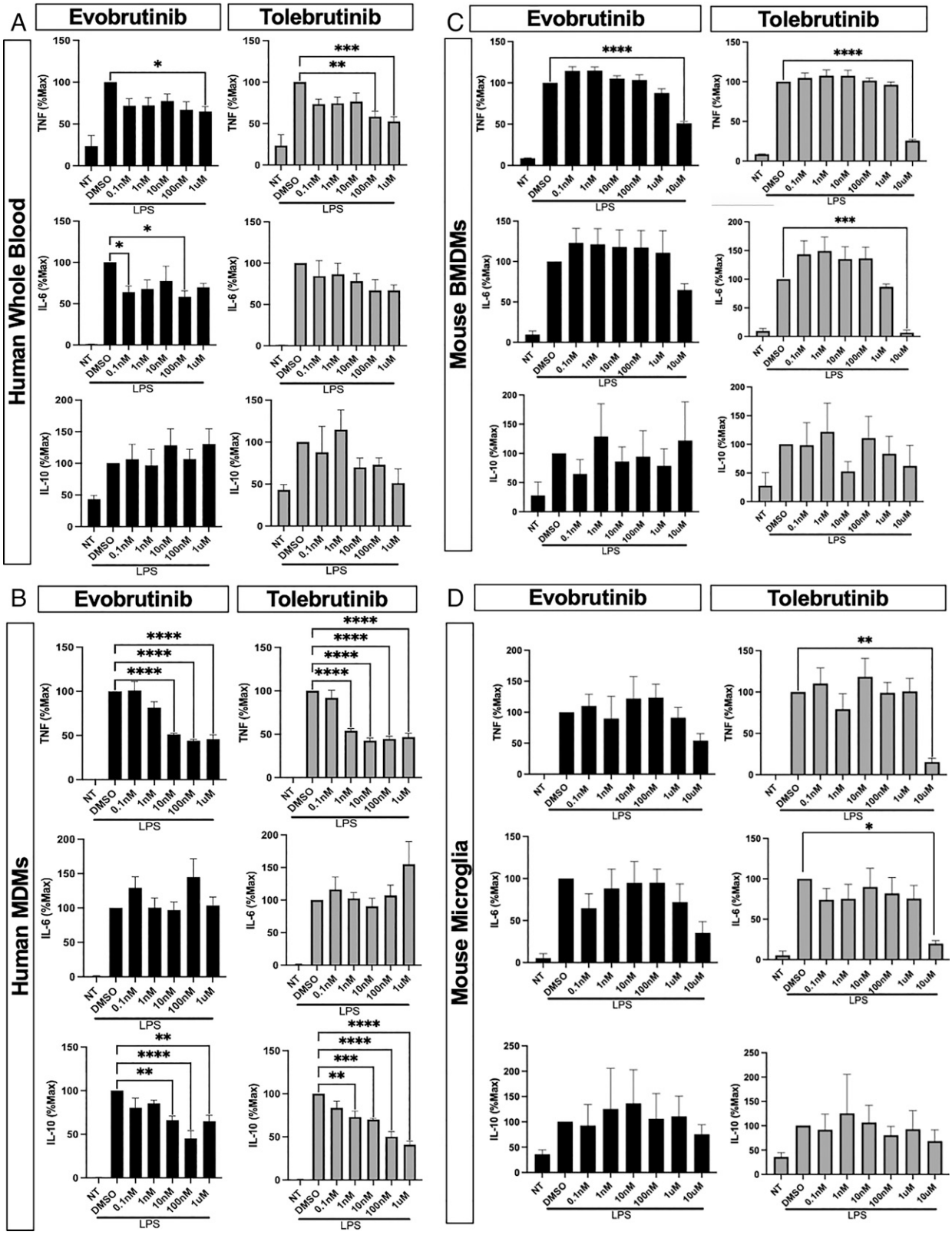

FIGURE 3. BTKis tolebrutinib and evobrutinib decrease cytokines in human and mouse myeloid cells.

(**A**) Tolebrutinib and evobrutinib significantly decreased TNF and IL-6 in human whole blood. (**B**) Tolebrutinib and evobrutinib significantly decreased TNF and IL-10 in human MDMs. (**C**) Tolebrutinib and evobrutinib significantly decreased TNF and IL-6 from mouse BMDMs. (**D**) Tolebrutinib significantly decreased TNF and IL-10 in mouse microglia (n = 6 per treatment per cell type). DMSO: 0.1% at 10 μM. Statistical analysis was ***(Continued)***

https://doi.org/10.4049/immunohorizons.2400045

measured cytokines in the supernatants of activated mouse macrophages and microglia. In BMDMs, a significant decrease in TNF and IL-6 levels was measured in the presence of tolebrutinib; a significant decrease in TNF was also measured in the presence of evobrutinib (Fig. 3C). In contrast with BMDMs, cytokine levels in activated microglia were not statistically decreased in the presence of evobrutinib, yet a trend was observed at higher doses. Tolebrutinib also significantly decreased TNF and IL-6 levels (Fig. 3D); no statistical differences were observed for IL-10.

Evobrutinib and tolebrutinib alter mitochondrial respiration in human and mouse myeloid cells

Using a Seahorse assay, a mito-stress test was used to measure OCR and ECAR. In human MDMs, evobrutinib significantly decreased both OCR and ECAR compared with LPS + DMSO control (Fig. 4A–D). In mouse BMDMs, evobrutinib also decreased OCR and ECAR (Fig. 4E–H). Decreased OCR and ECAR were also measured in mouse microglia in the presence of evobrutinib; however, the results were not statistically significant ($p = 0.292$; Fig. 4I–L). In contrast with evobrutinib, tolebrutinib did not significantly alter OCR but decreased ECAR compared to the LPS + DMSO control (Fig. 4M–P); a significant decrease in both OCR and ECAR was measured in BMDMs (Fig. 4Q–T). In mouse microglia, tolebrutinib decreased OCR, albeit not statistically significantly ($p = 0.084$), and a significant decrease in ECAR was measured (Fig. 4U–X).

Evobrutinib and tolebrutinib decrease phagocytosis in mouse myeloid cells

Using live-cell imaging and pHrodo zymosan beads, a phagocytosis assay was used to measure phagocytic activity in human and mouse myeloid cells in the presence of the BTKis. Data are represented in both real-time and peak fluorescence (i.e., phagocytosis) during the 6-h kinetic interval run. In human MDMs, no significant change in phagocytosis was measured between LPS alone and LPS plus evobrutinib at 80 min (Fig. 5A, 5B). In contrast, both mouse BMDMs and microglia had a decrease in phagocytosis in the presence of evobrutinib compared with LPS alone (Fig. 5C–F), yet results in microglia did not reach statistical significance. Similar results were observed with tolebrutinib (Fig. 5G–L).

Evobrutinib and tolebrutinib significantly decrease proinflammatory miRNAs in mouse myeloid cells

Using quantitative PCR, microRNA expression of proinflammatory miRNAs (miR-155-5p and miR-21-5p) and the anti-inflammatory miRNA (miR-223-3p) were measured in mouse myeloid cells. In mouse BMDMs, miR-155-5p and miR-21-5p were significantly decreased with both evobrutinib and tolebrutinib treatment (Fig. 6A); in mouse microglia, only miR-155-5p was significantly decreased (Fig. 6B). miR-223-3p expression trended upward in both mouse BMDMs and microglia with BTKi treatment; however, results were not statistically significant due to sample variability (Fig. 6A, 6B). Quantitative PCR assays were also performed in human MDMs; however, no conclusions could be made based on high intersample variability.

DISCUSSION

The importance of further elucidating and identifying the mechanism(s) of action for drugs that have entered late-stage clinical trials is critical to better understand their biological/cellular targets and any potential off-target effects within the human body. In MS, there are currently several disease-modifying therapies ranging from platform medications to moderate- and high-efficacy agents with various mechanisms of action. In this study, we undertook an investigation to expand the known mechanism of action of BTKis, a class of drugs that are being investigated in various immune-related conditions. Although there are several different BTKis currently being evaluated in clinical trials for both relapsing and progressive forms of MS, a further in-depth investigation into the mechanisms of evobrutinib and tolebrutinib was prioritized because these two drugs are furthest along in clinical trials and both cross the blood-brain barrier (BBB). All experiments performed in this study used myeloid cells derived from mouse and human to allow for interpretations based on any species-specific results. In summary, both evobrutinib and tolebrutinib decreased levels of p-BTK and cytokine expression in human and mouse myeloid cells under inflammatory states. In addition, both BTKis significantly influenced mitochondrial function, as reflected in measurable decreases in OCR and ECAR. Furthermore, the rates of phagocytosis were also shown to be influenced by BTKis, specifically in mouse-derived cells where the rate was significantly decreased. Finally, to further elucidate mechanisms, both BTKis altered miRNA expression profiles that mirrored an overall anti-inflammatory state. Taken together, our results confirm previous speculations and provide direct evidence that BTKis not only influence B cells, but can also act directly on myeloid cells and promote a CNS environment conducive for remyelination and repair.

Historically, BTKis have been used to effectively treat various B cell cancers, including CLL and MCL (31–34). In these malignancies, the mechanism(s) of action of BTKis on B cells is well understood, whereby they modulate B cell development, maturation, and proliferation (35, 36). Beyond cancers, recent clinical and preclinical data suggest that BTKis may also serve as an effective treatment for several autoimmune conditions, including MS, rheumatoid arthritis, and pemphigus vulgaris, with several early-stage and midstage clinical trials

performed using a one-way ANOVA with the main comparator group being DMSO + LPS. *$p < 0.05$, **$p < 0.01$, ***$p < 0.001$, ****$p < 0.0001$. Error bars represent mean ± SEM. NT, no treatment.

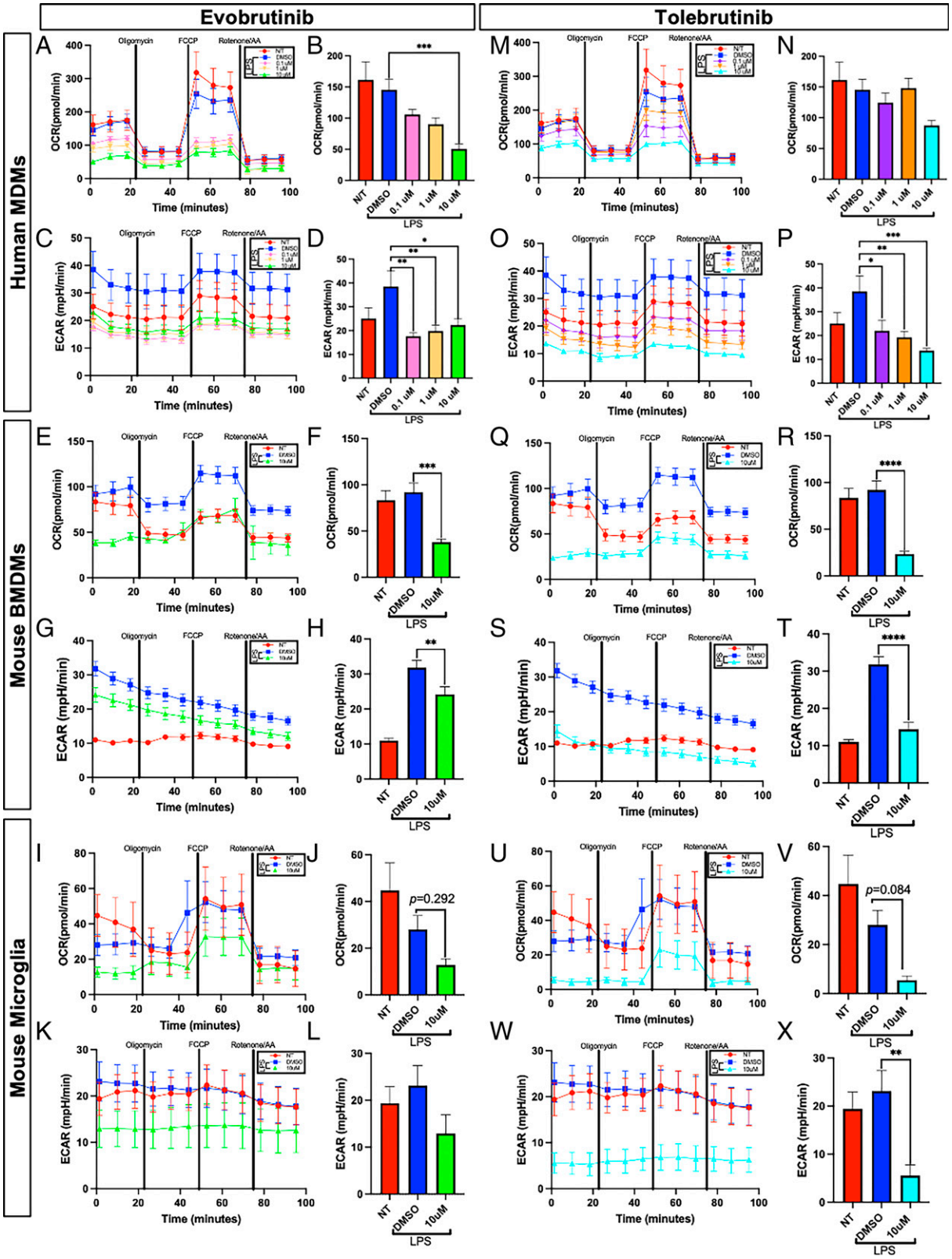

FIGURE 4. BTKis tolebrutinib and evobrutinib decrease OCR and ECAR in human MDMs and mouse BMDMs, but only ECAR in mouse microglia. (**A**–**L**) Evobrutinib influences OCR and ECAR under mito-stress test conditions and baseline functions in (A–D) human MDMs, (E–H) mouse BMDMs, and (I–L) microglia. (**M**–**X**) Tolebrutinib influences OCR and ECAR under mito-stress test conditions and baseline functions in (M–P) MDMs, (Q–T) BMDMs, and (U–X) microglia (n = 6 per treatment per cell type). DMSO: 0.1% at 10 μM. Statistical analysis was ***(Continued)***

https://doi.org/10.4049/immunohorizons.2400045

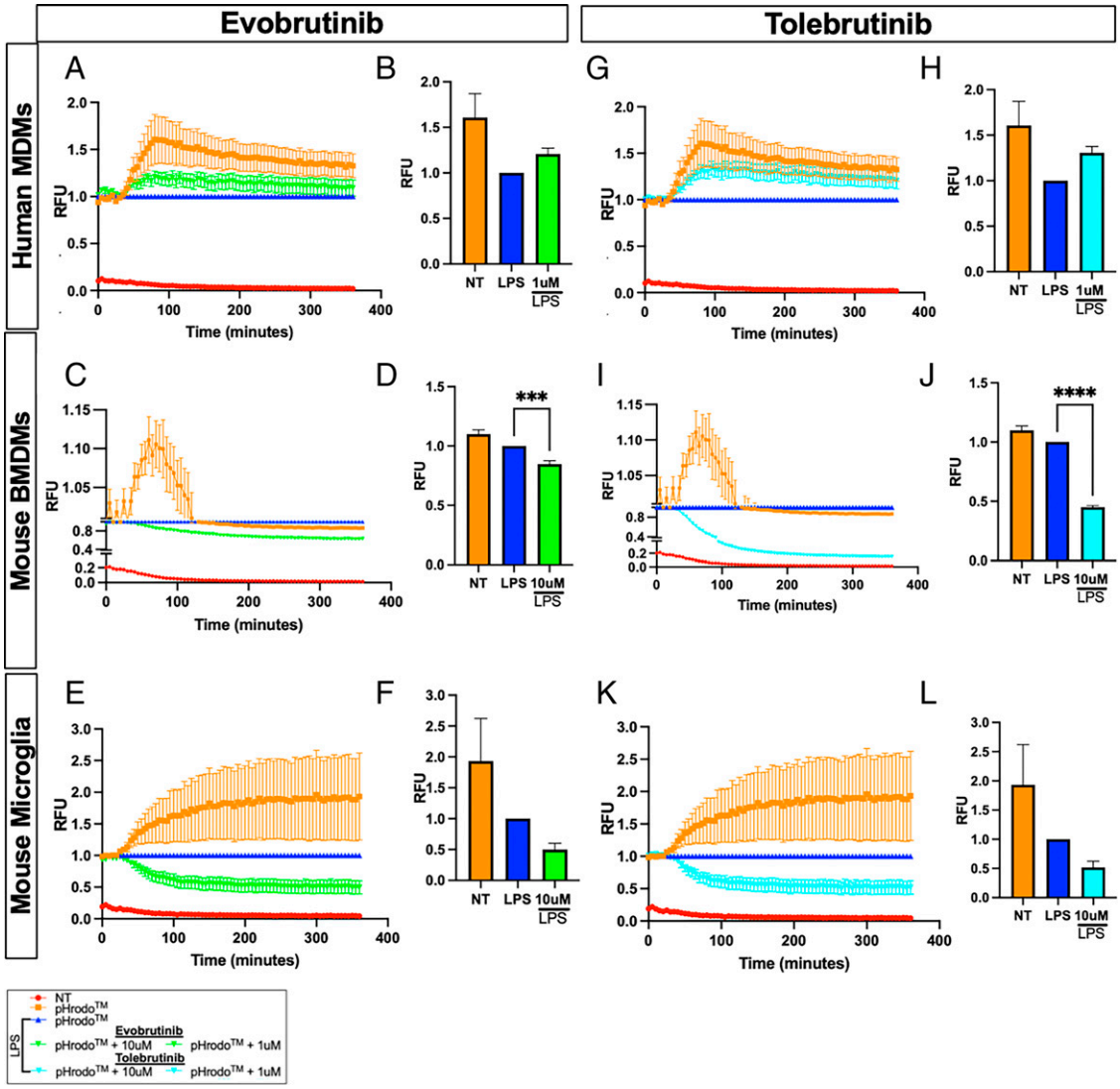

FIGURE 5. BTKis significantly decrease phagocytosis in mouse myeloid cells.

(**A**–**F**) Evobrutinib effects on normalized pHrodo Zymosan Bead fluorescence intensity in (A) human MDMs, (C) mouse BMDMs, and (E) microglia and the effects on pHrodo Zymosan Bead (pHrodo) fluorescence intensity at the end of a 6-h kinetic interval showing phagocytosis trending upward in (B) MDMs, but significantly decreasing in (D) BMDMs and (F) microglia. (**G**–**L**) Tolebrutinib effects on normalized pHrodo Zymosan Bead fluorescence intensity in (G) MDMs, (I) BMDMs, and (K) microglia and the effects on pHrodo Zymosan Bead (pHrodo) fluorescence intensity at the end of the 6-h kinetic interval showing phagocytosis trending upward in (H) MDMs, but significantly decreasing in (J) BMDMs and (L) microglia ($n = 6$ per treatment per cell type). Statistical analysis was performed using a one-way ANOVA with the main comparator group being DMSO + LPS. ***$p < 0.001$, ****$p < 0.0001$. Error bars represent mean ± SEM. NT, no treatment; pHrodo, zymosan beads only.

successfully meeting their primary end points (37–39). In the context of neurodegenerative diseases, two BTKis (tolebrutinib and evobrutinib) are currently being evaluated in phase 3 clinical trials in MS. Unlike some of the earlier investigated BTKis, both evobrutinib and tolebrutinib cross the BBB, thus making them among the first widely accepted BBB-penetrable drugs to treat MS (40, 41).

In MS, B cells play an important role in contributing to cellular processes involved in inflammation and degeneration within the CNS. Not only can B cells serve as APCs and differentiate into plasma cells that secrete Abs targeting various myelin and neuronal Ags, but their plasticity is also highly dependent on both the local microenvironment and immune-neural cross-talk that occurs within compartmentalized CNS inflammation (42, 43). In

performed using a one-way ANOVA with the main comparator group being DMSO + LPS. *$p < 0.05$, **$p < 0.01$, ***$p < 0.001$, ****$p < 0.0001$. Error bars represent mean ± SEM. NT, no treatment.

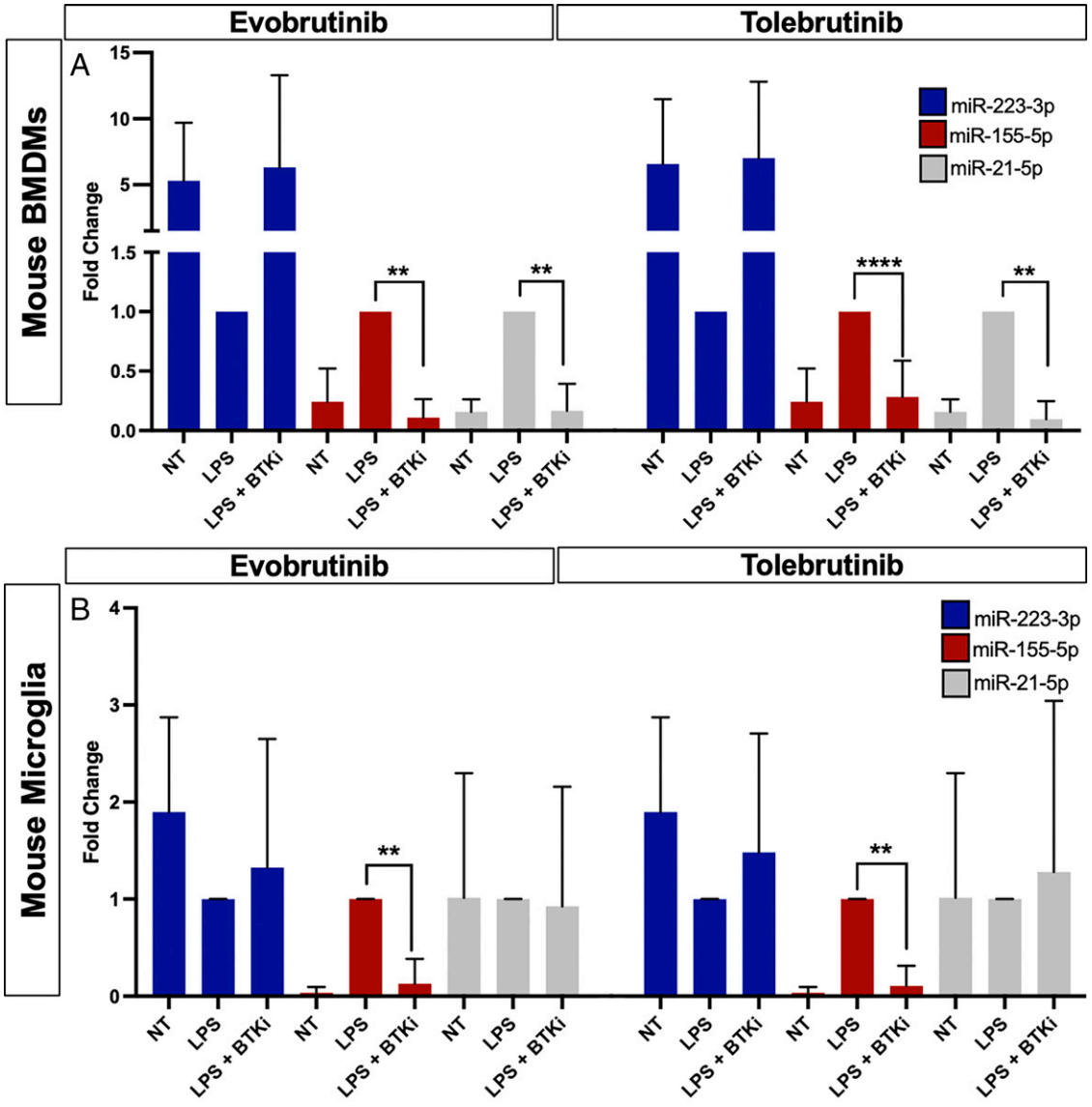

FIGURE 6. BTKis significantly decrease miRNA-155-5p in mouse BMDMs and microglia, and miRNA-21-5p in mouse BMDMs.
(**A**) Evobrutinib and tolebrutinib significantly decrease miR-155-5p and miR-21-5p in mouse BMDMs. (**B**) Evobrutinib and tolebrutinib significantly decrease miR-155-5p in mouse microglia. Mouse BMDMs: miR-223-3p and miR-21-5p; $n = 4$, miR-155-5p; $n = 6$; mouse microglia: miR-223-3p and miR-21-5p; $n = 5$, miR-155-5p; $n = 6$ (BTKi, 10 μM). Statistical analysis was performed using a one-way ANOVA with the main comparator group being LPS. $^{**}p < 0.01$, $^{****}p < 0.0001$. Error bars represent mean ± SEM.

the CNS of MS patients, the rich accumulation of B cells in tertiary follicle-like structures within the meningeal space leads to increased expression of proinflammatory cytokines that results in a graded inflammation, heightened microglia and astrocyte reactivity, neurodegeneration, and demyelination (44–47). As such, biologic therapies targeting B cells (e.g., anti-CD20 agents) have shown a high degree of efficacy in both relapsing and progressive forms of MS (48, 49).

In MS pathogenesis, an interconnected network of myeloid cells (e.g., monocytes, blood-derived macrophages, and microglia) and lymphocytes allows for cell-cell cross-talk between immune cells within the periphery and CNS, and contributes to inflammation, demyelination, and neuronal/axonal degeneration (50–56). To date, the majority of disease-modifying therapies have largely focused on targeting the proinflammatory actions of both T and B lymphocytes. However, it has become increasingly acknowledged that myeloid cells also play a critical role in not only activating innate and adaptive immune responses and serving as efficient APCs (57, 58) but also play a role in the early recognition of pathogens, including those that have been linked to MS (e.g., EBV and herpes viruses) (59–61). In addition, the slowly expanding lesions in MS, which are characterized by an active iron-laden microglia/macrophage border, have been associated with disease progression and brain atrophy in several

https://doi.org/10.4049/immunohorizons.2400045

pathological and imaging studies, thereby suggesting that targeting these cells may have profound effects on the trajectory and disease course in MS (62–64). A recent study by Steinmaurer et al. (65) demonstrated that BTK expression was directly associated with iron accumulation within myeloid cells in MS, suggesting that targeting BTK within the CNS may significantly alter disease course. In addition, a study by Geladaris et al. (30) also demonstrated that BTK inhibition can decrease microglia-related inflammation and promote myelin repair.

Although initially overlooked, the expression of *btk* within myeloid cells is considerable and indeed comparable with B cells (66). In addition, because downstream signaling pathways mediated by BTK are similar in B cells and myeloid cells (67–70), a further investigation into how BTK inhibition is directly altering the function of myeloid cells is warranted. Taken together, the diverse roles and plasticity of myeloid-derived cells within the inflamed CNS has led to research aimed at further understanding how the phenotype and function of these cells can be altered to halt inflammation and provide an opportunity to promote remyelination and repair. In this study, the direct effects of BTK inhibition on the phenotype and function of both human and mouse myeloid cells in the context inflammatory-mediated CNS injury were explored. Given the known effects of BTKis on B cells, it was hypothesized that BTKis would also decrease the inflammatory phenotype of both peripheral and central myeloid cells by modulating proinflammatory cytokine profiles, miRNA expression, bioenergetics and cell metabolism, and phagocytic capacity.

In clinical trials, a daily dosing regimen of tolebrutinib (7.5–90 mg) results in a mean plasma concentration between 1.17 and 19.3 ng/ml (or 0.002 and 0.4 μM) (71); a dose of 25–500 mg of evobrutinib results in a plasma concentration between 181 and 465 ng/ml (or 0.42 and 1.08 μM) (72). Taking these levels into consideration, a broad range of doses between 0.1 nM and 10 μM of both inhibitors (tolebrutinib [IC_{50} = 0.7 nM] and evobrutinib [IC_{50} = 37.9 nM]) was applied to human and mouse cells in our study. LPS, a potent activator of TLR4 that increases BTK-mediated signaling, was used to induce an inflammatory response in human MDMs, mouse BMDMs, and microglia (73, 74). To confirm the mechanistic function of both BTKis, we performed quantification of p-BTK via ELISA and ICC (Figs. 1, 2). These results demonstrated that both BTKis significantly decreased p-BTK in human and mouse myeloid cells. In human MDMs, p-BTK was significantly decreased at 1 and 10 μM; in mouse BMDMs and microglia, p-BTK was significantly decreased at 10 μM. Although no significant decrease in p-BTK was observed in mouse microglia treated with evobrutinib using ICC (Fig. 1F), a decrease in total p-BTK protein was measured via ELISA.

After confirmation of reduced p-BTK with the application of BTKis, different downstream effects were evaluated, including cytokine production. TLR4 activation plays a functional role in the transcription of NF-κB, which results in the production of various cytokines, including TNF, IL-6, and IL-10 (73). To understand how BTKis function in human cells in vitro, both whole blood and MDMs were used. In human whole blood, a significant decrease in TNF and IL-6 was observed in the presence of a BTKi after LPS stimulation. Because whole blood contains granulocytes (which also express high levels of BTK), monocytes, and lymphocytes, these results may be due, in part, to an effect of the BTKis with any or all of these cells. To investigate a macrophage-specific response, we activated human MDMs in the presence of the BTKis. Both IL-10 and TNF levels were decreased, but not IL-6 (Fig. 3B). This result is consistent with previous literature suggesting that BTK is required for TLR4-induced TNF production, but not IL-6, whereby no differences in *il6* mRNA were measured in primary macrophages derived from both XLA (BTK deficient) and healthy controls (4). Interestingly, IL-6 was significantly decreased in TLR2-activated XLA macrophages (4).

According to the published literature, species-specific effects have been observed between mice and humans (in vitro and in vivo) in terms of differently responding to BTKis (75). It was therefore important to investigate any differences between species when measuring the cellular responses in the presence of tolebrutinib or evobrutinib. Our results demonstrated that tolebrutinib significantly decreased both TNF and IL-6, yet only TNF was decreased in BMDMs in the presence of evobrutinib. The small effect observed in mouse cells treated with evobrutinib was not surprising, because mouse models of colorectal cancer and SARS-CoV-2– or LPS-induced lung damage have shown that evobrutinib does not effectively target BTK or decrease disease (76). Taken together, tolebrutinib and evobrutinib similarly decreased TNF and IL-6 in human whole blood and TNF and IL-10 in MDMs; however, tolebrutinib was superior at decreasing TNF and IL-6 in mouse-derived myeloid cells.

Inflammation and mitochondrial dysfunction are often associated with one another, whereby decreasing inflammation often results in an overall increase in mitochondrial health (77–79). In autoimmune diseases, various cell types (PBMCs, endothelial, mesangial, fibroblasts) have been demonstrated to alter their bioenergetic profiles, including the cellular mechanisms involved in producing and maintaining energy. Mitochondrial dysfunction has been noted in many diseases whereby mitochondrial respiration within impacted cells is less efficient compared with cells derived from their healthy counterparts (80–83). Specifically, in neurodegenerative diseases that are driven by inflammation, mitochondrial dysfunction has been observed, but not limited to, in Alzheimer's disease, Parkinson's disease, and MS (84–87). In the well-established MS mouse model, experimental autoimmune encephalomyelitis, it has been shown that increasing the number of mitochondria and expanding the respiratory rate in mitochondria results in less CNS inflammation and allows for better recovery (87).

A standard technique for measuring cellular respiration, both OCRs and ECARs quantify oxygen requirements and the rate of glycolysis through quantifying changes in dissolved oxygen and pH within the media surrounding live cells (88). When exposed to proinflammatory stimuli, myeloid cells undergo a metabolic switch favoring glycolysis, thereby reducing oxidative phosphorylation (89, 90). In our experiments, LPS resulted in a direct

increase in ECAR in both human and mouse myeloid cells (Fig. 4); a direct shift in mitochondrial metabolism within human or mouse cells treated with BTKis was not observed, whereby OCR and ECAR decreased in the presence of BTKis after exposure to LPS (Fig. 4). Recently, the perspective on the "metabolic switch" describing mitochondrial function during inflammation has been suggested to be more complex. Specifically, the notion that cells do not necessarily fully take on a preferential role for oxidative phosphorylation over glycolysis (and vice versa) has been challenged (91). A single glucose molecule is enzymatically converted to two ATP molecules, and in conditions of reduced glycolysis (reduced ECAR), the phosphate equivalents are processed twice, which results in phosphorylation of ADP, not ATP, at the substrate level (92). The observed decrease in ECAR suggests that BTKis permit cells to be "less glycolytic" during LPS-induced inflammation, whereas the observed decrease in OCR suggests that BTKis can lower the oxygen requirement for ATP production under the same conditions (93). These results are in contrast with previous work, whereby inhibition of BTK in macrophages from patients with atherosclerosis resulted in a direct shift to use oxidative phosphorylation and increase mitochondrial stress (94). Together, these findings suggest that the BTKis are able to alter the metabolism of human and mouse myeloid cells in a manner that energy can still be produced, yet the mitochondria do not exhibit a distinct shift between oxidative phosphorylation and glycolytic phenotypes.

Understanding the effect of BTKis on phagocytosis in both peripheral and central macrophages is important because it is the primary mechanism and initial step to rid the body of invading pathogens, including viruses and bacteria (95). In addition, the efficiency of phagocytosis is also critical when clearing cellular debris postinjury, thus creating space for regeneration and/or remyelination (96–100). In our experiments, a species-related difference was observed in the rate of phagocytosis in the presence of either evobrutinib or tolebrutinib (Fig. 5). In human MDMs, the rate of phagocytosis trended upward with BTKi treatment; phagocytosis rates decreased in mouse myeloid cells. BTK is required for mouse macrophages to efficiently perform phagocytosis (28, 101, 102). In the context of cancer, a role for BTK in phagocytosis has been previously shown whereby different BTKis can either increase or decrease phagocytosis in macrophages derived from cancer patients (103, 104). It is therefore surprising that the BTKis did not alter phagocytosis in the human MDMs, yet it is important to note that our experiments used MDMs derived from healthy individuals. Furthermore, the study mentioned earlier used a different BTKi, ibrutinib. There are currently no studies using evobrutinib or tolebrutinib to measure the rate of phagocytosis in human MDMs. Our results therefore suggest that different BTKis (which have different IC_{50}s) may result in differential mechanisms during infection and/or injury. Both BTKis show promise at increasing the rate of phagocytosis in human MDMs, which has been previously shown in cancer (103).

Investigating the role of BTKis in terms of miRNA modulation provides mechanistic insight into how the inhibitors are causing myeloid cells to respond in an anti-inflammatory versus proinflammatory manner. The proinflammatory miR-155-5p and miR-21-5p and anti-inflammatory miR-223-3p were chosen because they have been shown to have differential effects during diseased states. miR-155-5p and miR-21-5p have been shown to be associated with a proinflammatory phenotype in macrophages and microglia (105–107) and have been shown to enhance CNS inflammation and promote neural injury in both humans and mice (108–110). In the CNS, miR-223-3p has been shown to promote a reparative and anti-inflammatory phenotype in human and mouse myeloid cells (111, 112). Taking these factors into consideration, the role of BTKis and miRNA expression was explored to determine whether BTK inhibition would alter miRNA expression in human and mouse myeloid cells. Mouse BMDMs and microglia both showed a significant decrease in miR-155-5p in the presence of LPS and BTKi, whereas only BMDMs showed a significant decrease in miR-21-5p (Fig. 6). Although miR-223-3p trended toward an increase, the variation within the individual groups did not provide statistically significant results (Fig. 6). Exploring the effects of BTK inhibition and miRNA production is yet another important mechanism to explore how BTKis can influence the function and phenotype of myeloid cells.

In summary, our results provide important insights into further establishing the mechanism of action of BTKis and their direct effects on both mouse and human myeloid cells. Taken together, this data contributes to the growing field of BTK inhibition within a myeloid cell context and provides further rationale to support the clinical use of these drugs in the treatment of neuroinflammatory conditions.

DISCLOSURES

The authors have no financial conflicts of interest.

ACKNOWLEDGMENTS

We thank Tangyne Berry and Neva Fudge for technical assistance. We also dedicate this work in memory of James (Jimmy) Benoit.

REFERENCES

1. Yang, Y., J. Shi, Z. Gu, M. E. Salama, S. Das, E. Wendlandt, H. Xu, J. Huang, Y. Tao, M. Hao, et al. 2015. Bruton tyrosine kinase is a therapeutic target in stem-like cells from multiple myeloma. *Cancer Res.* 75: 594–604.
2. Marcotte, D. J., Y. Liu, R. M. Arduini, C. A. Hession, K. Miatkowski, C. P. Wildes, P. F. Cullen, V. Hong, B. T. Hopkins, E. Mertsching, et al. 2010. Structures of human Bruton's tyrosine kinase in active and inactive conformations suggest a mechanism of activation for TEC family kinases. *Protein Sci.* 19: 429–439.
3. Simonowski, A., T. Wilhelm, P. Habib, C. N. Zorn, and M. Huber. 2020. Differential use of BTK and PLC in FcεRI- and KIT-mediated

mast cell activation: a marginal role of BTK upon KIT activation. *Biochim. Biophys. Acta Mol. Cell. Res.* 1867: 118622.
4. Horwood, N. J., T. H. Page, J. P. McDaid, C. D. Palmer, J. Campbell, T. Mahon, F. M. Brennan, D. Webster, and B. M. J. Foxwell. 2006. Bruton's tyrosine kinase is required for TLR2 and TLR4-induced TNF, but not IL-6, production. *J. Immunol.* 176: 3635–3641.
5. Doyle, S. L., C. A. Jefferies, C. Feighery, and L. A. O'Neill. 2007. Signaling by Toll-like receptors 8 and 9 requires Bruton's tyrosine kinase. *J. Biol. Chem.* 282: 36953–36960.
6. Chen, S.-S., B. Y. Chang, S. Chang, T. Tong, S. Ham, B. Sherry, J. A. Burger, K. R. Rai, and N. Chiorazzi. 2016. BTK inhibition results in impaired CXCR4 chemokine receptor surface expression, signaling and function in chronic lymphocytic leukemia. *Leukemia* 30: 833–843.
7. Park, H., M. I. Wahl, D. E. H. Afar, C. W. Turck, D. J. Rawlings, C. Tam, A. M. Scharenberg, J.-P. Kinet, and O. N. Witte. 1996. Regulation of Btk function by a major autophosphorylation site within the SH3 domain. *Immunity* 4: 515–525.
8. Hyvönen, M., and M. Saraste. 1997. Structure of the PH domain and Btk motif from Bruton's tyrosine kinase: molecular explanations for X-linked agammaglobulinaemia. *EMBO J.* 16: 3396–3404.
9. Pellerin, K., S. J. Rubino, J. C. Burns, B. A. Smith, C.-A. McCarl, J. Zhu, L. Jandreski, P. Cullen, T. M. Carlile, A. Li, et al. 2021. MOG autoantibodies trigger a tightly-controlled FcR and BTK-driven microglia proliferative response. *Brain* 144: 2361–2374.
10. Crespo, O., S. C. Kang, R. Daneman, T. M. Lindstrom, P. P. Ho, R. A. Sobel, L. Steinman, and W. H. Robinson. 2011. Tyrosine kinase inhibitors ameliorate autoimmune encephalomyelitis in a mouse model of multiple sclerosis. *J. Clin. Immunol.* 31: 1010–1020.
11. Menzfeld, C., M. John, D. van Rossum, T. Regen, J. Scheffel, H. Janova, A. Götz, S. Ribes, R. Nau, A. Borisch, et al. 2015. Tyrphostin AG126 exerts neuroprotection in CNS inflammation by a dual mechanism. *Glia* 63: 1083–1099.
12. Murali, I., S. Kasar, A. Naeem, S. Tyekucheva, J. K. Khalsa, E. M. Thrash, G. Itchaki, D. Livitz, I. Leshchiner, S. Dong, et al. 2021. Activation of the MAPK pathway mediates resistance to PI3K inhibitors in chronic lymphocytic leukemia. *Blood* 138: 44–56.
13. Smith, C. I., B. Baskin, P. Humire-Greiff, J. N. Zhou, P. G. Olsson, H. S. Maniar, P. Kjellén, J. D. Lambris, B. Christensson, L. Hammarström, et al. 1994. Expression of Bruton's agammaglobulinemia tyrosine kinase gene, BTK, is selectively down-regulated in T lymphocytes and plasma cells. *J. Immunol.* 152: 557–565.
14. Vetrie, D., I. Vorechovský, P. Sideras, J. Holland, A. Davies, F. Flinter, L. Hammarström, C. Kinnon, R. Levinsky, M. Bobrow, et al. 1993. The gene involved in X-linked agammaglobulinaemia is a member of the src family of protein-tyrosine kinases. *Nature* 361: 226–233.
15. Hendriks, R. W., S. Yuvaraj, and L. P. Kil. 2014. Targeting Bruton's tyrosine kinase in B cell malignancies. *Nat. Rev. Cancer* 14: 219–232.
16. Byrd, J. C., R. R. Furman, S. E. Coutre, I. W. Flinn, J. A. Burger, K. A. Blum, B. Grant, J. P. Sharman, M. Coleman, W. G. Wierda, et al. 2013. Targeting BTK with ibrutinib in relapsed chronic lymphocytic leukemia. *N. Engl. J. Med.* 369: 32–42.
17. Burger, J. A., A. Tedeschi, P. M. Barr, T. Robak, C. Owen, P. Ghia, O. Bairey, P. Hillmen, N. L. Bartlett, J. Li, et al.; RESONATE-2 Investigators. 2015. Ibrutinib as initial therapy for patients with chronic lymphocytic leukemia. *N. Engl. J. Med.* 373: 2425–2437.
18. Estupiñán, H. Y., A. Berglöf, R. Zain, and C. I. E. Smith. 2021. Comparative analysis of BTK inhibitors and mechanisms underlying adverse effects. *Front. Cell. Dev. Biol.* 9: 630942.
19. Good, L., B. Benner, and W. E. Carson. 2021. Bruton's tyrosine kinase: an emerging targeted therapy in myeloid cells within the tumor microenvironment. *Cancer Immunol. Immunother.* 70: 2439–2451.
20. Stiff, A., P. Trikha, R. Wesolowski, K. Kendra, V. Hsu, S. Uppati, E. McMichael, M. Duggan, A. Campbell, K. Keller, et al. 2016. Myeloid-derived suppressor cells express Bruton's tyrosine kinase and can be depleted in tumor-bearing hosts by ibrutinib treatment. *Cancer Res.* 76: 2125–2136.
21. Ping, L., N. Ding, Y. Shi, L. Feng, J. Li, Y. Liu, Y. Lin, C. Shi, X. Wang, Z. Pan, et al. 2017. The Bruton's tyrosine kinase inhibitor ibrutinib exerts immunomodulatory effects through regulation of tumor-infiltrating macrophages. *Oncotarget* 8: 39218–39229.
22. De Bondt, M., J. Renders, S. Struyf, and N. Hellings. 2024. Inhibitors of Bruton's tyrosine kinase as emerging therapeutic strategy in autoimmune diseases. *Autoimmun. Rev.* 23: 103532.
23. Sharma, M. D., R. Pacholczyk, H. Shi, Z. J. Berrong, Y. Zakharia, A. Greco, C.-S. S. Chang, S. Eathiraj, E. Kennedy, T. Cash, et al. 2021. Inhibition of the BTK-IDO-mTOR axis promotes differentiation of monocyte-lineage dendritic cells and enhances anti-tumor T cell immunity. *Immunity* 54: 2354–2371.e8.
24. Bhargava, P., S. Kim, A. A. Reyes, R. Grenningloh, U. Boschert, M. Absinta, C. Pardo, P. Van Zijl, J. Zhang, P. A. Calabresi, et al. 2021. Imaging meningeal inflammation in CNS autoimmunity identifies a therapeutic role for BTK inhibition. *Brain* 144: 1396–1408.
25. de Porto, A. P., Z. Liu, R. de Beer, S. Florquin, J. J. T. H. Roelofs, O. J. de Boer, J. M. M. den Haan, R. W. Hendriks, C. van 't Veer, T. van der Poll, et al. 2021. Bruton's tyrosine kinase-mediated signaling in myeloid cells is required for protective innate immunity during pneumococcal pneumonia. *Front. Immunol.* 12: 723967.
26. Evonuk, K. S., S. Wang, J. Mattie, C. J. Cracchiolo, R. Mager, Ž. Ferenčić, E. Sprague, B. Carrier, K. Schofield, E. Martinez, et al. 2023. Bruton's tyrosine kinase inhibition reduces disease severity in a model of secondary progressive autoimmune demyelination. *Acta Neuropathol. Commun.* 11: 115.
27. Liu, Y., Z. Huang, T.-X. Zhang, B. Han, G. Yang, D. Jia, L. Yang, Q. Liu, A. Y. L. Lau, F. Paul, et al. 2023. Bruton's tyrosine kinase-bearing B cells and microglia in neuromyelitis optica spectrum disorder. *J. Neuroinflammation* 20: 309.
28. Keaney, J., J. Gasser, G. Gillet, D. Scholz, and I. Kadiu. 2019. Inhibition of Bruton's tyrosine kinase modulates microglial phagocytosis: therapeutic implications for Alzheimer's disease. *J. Neuroimmune Pharmacol.* 14: 448–461.
29. Nam, H. Y., J. H. Nam, G. Yoon, J.-Y. Lee, Y. Nam, H.-J. Kang, H.-J. Cho, J. Kim, and H.-S. Hoe. 2018. Ibrutinib suppresses LPS-induced neuroinflammatory responses in BV2 microglial cells and wild-type mice. *J. Neuroinflammation* 15: 271.
30. Geladaris, A., S. Torke, D. Saberi, Y. B. Alankus, F. Streit, S. Zechel, C. Stadelmann-Nessler, A. Fischer, U. Boschert, D. Häusler, et al. 2024. BTK inhibition limits microglia-perpetuated CNS inflammation and promotes myelin repair. *Acta Neuropathol.* 147: 75.
31. Zelenetz, A. D., L. I. Gordon, J. S. Abramson, R. H. Advani, B. Andreadis, N. L. Bartlett, L. E. Budde, P. F. Caimi, J. E. Chang, B. Christian, et al. 2023. NCCN Guidelines(R) insights: B-cell lymphomas, version 6.2023. *J. Natl Compr. Canc. Netw.* 21: 1118–1131.
32. Sun, C., P. Nierman, E. K. Kendall, J. Cheung, M. Gulrajani, S. E. M. Herman, C. Pleyer, I. E. Ahn, M. Stetler-Stevenson, C. M. Yuan, et al. 2020. Clinical and biological implications of target occupancy in CLL treated with the BTK inhibitor acalabrutinib. *Blood* 136: 93–105.
33. Song, Y., K. Zhou, D. Zou, J. Zhou, J. Hu, H. Yang, H. Zhang, J. Ji, W. Xu, J. Jin, et al. 2022. Zanubrutinib in relapsed/refractory mantle cell lymphoma: long-term efficacy and safety results from a phase 2 study. *Blood* 139: 3148–3158.
34. Raedler, L. A. 2015. Imbruvica (ibrutinib), first-in-class Bruton's tyrosine kinase inhibitor, receives expanded indications for patients with relapsed chronic lymphocytic leukemia. *Am. Health Drug Benefits* 8: 66–69.
35. Nyhoff, L. E., A. S. Griffith, E. S. Clark, J. W. Thomas, W. N. Khan, and P. L. Kendall. 2021. Btk supports autoreactive B cell development and protects against apoptosis but is expendable for antigen presentation. *J. Immunol.* 207: 2922–2932.

36. Smith, C. I. E., and J. A. Burger. 2021. Resistance mutations to BTK inhibitors originate from the NF-κB but not from the PI3K-RAS-MAPK arm of the B cell receptor signaling pathway. *Front. Immunol.* 12: 689472.
37. Conaghan, P. G., M. Nowak, S. Du, Y. Luo, J. Landis, C. Pachai, A. Fura, I. M. Catlett, D. M. Grasela, M. Østergaard, et al. 2023. Evaluation of BMS-986142, a reversible Bruton's tyrosine kinase inhibitor, for the treatment of rheumatoid arthritis: a phase 2, randomised, double-blind, dose-ranging, placebo-controlled, adaptive design study. *Lancet Rheumatol.* 5: e263–e273.
38. Murrell, D. F., A. Patsatsi, P. Stavropoulos, S. Baum, T. Zeeli, J. S. Kern, A.-V. Roussaki-Schulze, R. Sinclair, I. D. Bassukas, D. Thomas, et al.; BELIEVE trial investigators. 2021. Proof of concept for the clinical effects of oral rilzabrutinib, the first Bruton tyrosine kinase inhibitor for pemphigus vulgaris: the phase II BELIEVE study. *Br. J. Dermatol.* 185: 745–755.
39. Ringheim, G. E., M. Wampole, and K. Oberoi. 2021. Bruton's tyrosine kinase (BTK) inhibitors and autoimmune diseases: making sense of BTK inhibitor specificity profiles and recent clinical trial successes and failures. *Front. Immunol.* 12: 662223.
40. Reich, D. S., D. L. Arnold, P. Vermersch, A. Bar-Or, R. J. Fox, A. Matta, T. Turner, E. Wallström, X. Zhang, M. Mareš, et al.; Tolebrutinib Phase 2b Study Group. 2021. Safety and efficacy of tolebrutinib, an oral brain-penetrant BTK inhibitor, in relapsing multiple sclerosis: a phase 2b, randomised, double-blind, placebo-controlled trial. *Lancet Neurol.* 20: 729–738.
41. Montalban, X., K. Piasecka-Stryczynska, J. Kuhle, P. Benkert, D. L. Arnold, M. S. Weber, A. Seitzinger, H. Guehring, J. Shaw, D. Tomic, et al. 2024. Efficacy and safety results after >3.5 years of treatment with the Bruton's tyrosine kinase inhibitor evobrutinib in relapsing multiple sclerosis: long-term follow-up of a phase II randomised clinical trial with a cerebrospinal fluid sub-study. *Mult. Scler.* 30: 558–570.
42. Touil, H., R. Li, L. Zuroff, C. S. Moore, L. Healy, F. Cignarella, L. Piccio, S. Ludwin, A. Prat, J. Gommerman, et al. 2023. Cross-talk between B cells, microglia and macrophages, and implications to central nervous system compartmentalized inflammation and progressive multiple sclerosis. *EBioMedicine* 96: 104789.
43. Michel, L., C. Grasmuck, M. Charabati, M.-A. Lécuyer, S. Zandee, T. Dhaeze, J. I. Alvarez, R. Li, S. Larouche, L. Bourbonnière, et al. 2019. Activated leukocyte cell adhesion molecule regulates B lymphocyte migration across central nervous system barriers. *Sci. Transl. Med.* 11: eaaw0475.
44. Serafini, B., B. Rosicarelli, R. Magliozzi, E. Stigliano, and F. Aloisi. 2004. Detection of ectopic B-cell follicles with germinal centers in the meninges of patients with secondary progressive multiple sclerosis. *Brain Pathol.* 14: 164–174.
45. Magliozzi, R., O. Howell, A. Vora, B. Serafini, R. Nicholas, M. Puopolo, R. Reynolds, and F. Aloisi. 2007. Meningeal B-cell follicles in secondary progressive multiple sclerosis associate with early onset of disease and severe cortical pathology. *Brain* 130: 1089–1104.
46. Howell, O. W., E. K. Schulz-Trieglaff, D. Carassiti, S. M. Gentleman, R. Nicholas, F. Roncaroli, and R. Reynolds. 2015. Extensive grey matter pathology in the cerebellum in multiple sclerosis is linked to inflammation in the subarachnoid space. *Neuropathol. Appl. Neurobiol.* 41: 798–813.
47. Absinta, M., D. Maric, M. Gharagozloo, T. Garton, M. D. Smith, J. Jin, K. C. Fitzgerald, A. Song, P. Liu, J.-P. Lin, et al. 2021. A lymphocyte-microglia-astrocyte axis in chronic active multiple sclerosis. *Nature* 597: 709–714.
48. Kappos, L., J. S. Wolinsky, G. Giovannoni, D. L. Arnold, Q. Wang, C. Bernasconi, F. Model, H. Koendgen, M. Manfrini, S. Belachew, et al. 2020. Contribution of relapse-independent progression vs relapse-associated worsening to overall confirmed disability accumulation in typical relapsing multiple sclerosis in a pooled analysis of 2 randomized clinical trials. *JAMA Neurol.* 77: 1132–1140.
49. Gärtner, J., S. L. Hauser, A. Bar-Or, X. Montalban, J. A. Cohen, A. H. Cross, K. Deiva, H. Ganjgahi, D. A. Häring, B. Li, et al. 2022. Efficacy and safety of ofatumumab in recently diagnosed, treatment-naive patients with multiple sclerosis: results from ASCLEPIOS I and II. *Mult. Scler.* 28: 1562–1575.
50. Bennett, M. L., F. C. Bennett, S. A. Liddelow, B. Ajami, J. L. Zamanian, N. B. Fernhoff, S. B. Mulinyawe, C. J. Bohlen, A. Adil, A. Tucker, et al. 2016. New tools for studying microglia in the mouse and human CNS. *Proc. Natl Acad. Sci. USA* 113: E1738–E1746.
51. Hagemeyer, N., K.-M. Hanft, M.-A. Akriditou, N. Unger, E. S. Park, E. R. Stanley, O. Staszewski, L. Dimou, and M. Prinz. 2017. Microglia contribute to normal myelinogenesis and to oligodendrocyte progenitor maintenance during adulthood. *Acta Neuropathol.* 134: 441–458.
52. Paterka, M., J. O. Voss, J. Werr, E. Reuter, S. Franck, T. Leuenberger, J. Herz, H. Radbruch, T. Bopp, V. Siffrin, et al. 2017. Dendritic cells tip the balance towards induction of regulatory T cells upon priming in experimental autoimmune encephalomyelitis. *J. Autoimmun.* 76: 108–114.
53. Peferoen, L. A. N., D. Y. S. Vogel, K. Ummenthum, M. Breur, P. D. A. M. Heijnen, W. H. Gerritsen, R. M. B. Peferoen-Baert, P. van der Valk, C. D. Dijkstra, S. Amor, et al. 2015. Activation status of human microglia is dependent on lesion formation stage and remyelination in multiple sclerosis. *J. Neuropathol. Exp. Neurol.* 74: 48–63.
54. Poliani, P. L., Y. Wang, E. Fontana, M. L. Robinette, Y. Yamanishi, S. Gilfillan, and M. Colonna. 2015. TREM2 sustains microglial expansion during aging and response to demyelination. *J. Clin. Invest.* 125: 2161–2170.
55. Pham, T. H. M., P. Baluk, Y. Xu, I. Grigorova, A. J. Bankovich, R. Pappu, S. R. Coughlin, D. M. McDonald, S. R. Schwab, J. G. Cyster, et al. 2010. Lymphatic endothelial cell sphingosine kinase activity is required for lymphocyte egress and lymphatic patterning. *J. Exp. Med.* 207: 17–27.
56. Schläger, C., H. Körner, M. Krueger, S. Vidoli, M. Haberl, D. Mielke, E. Brylla, T. Issekutz, C. Cabañas, P. J. Nelson, et al. 2016. Effector T-cell trafficking between the leptomeninges and the cerebrospinal fluid. *Nature* 530: 349–353.
57. Ifergan, I., and S. D. Miller. 2020. Potential for targeting myeloid cells in controlling CNS inflammation. *Front. Immunol.* 11: 571897.
58. Jakhmola, S., M. F. Sk, A. Chatterjee, K. Jain, P. Kar, and H. C. Jha. 2022. A plausible contributor to multiple sclerosis; presentation of antigenic myelin protein epitopes by major histocompatibility complexes. *Comput. Biol. Med.* 148: 105856.
59. Lanz, T. V., R. C. Brewer, P. P. Ho, J.-S. Moon, K. M. Jude, D. Fernandez, R. A. Fernandes, A. M. Gomez, G.-S. Nadj, C. M. Bartley, et al. 2022. Clonally expanded B cells in multiple sclerosis bind EBV EBNA1 and GlialCAM. *Nature* 603: 321–327.
60. Bjornevik, K., M. Cortese, B. C. Healy, J. Kuhle, M. J. Mina, Y. Leng, S. J. Elledge, D. W. Niebuhr, A. I. Scher, K. L. Munger, et al. 2022. Longitudinal analysis reveals high prevalence of Epstein-Barr virus associated with multiple sclerosis. *Science* 375: 296–301.
61. Arvin, A. M., J. S. Wolinsky, L. Kappos, M. I. Morris, A. T. Reder, C. Tornatore, A. Gershon, M. Gershon, M. J. Levin, M. Bezuidenhoudt, et al. 2015. Varicella-zoster virus infections in patients treated with fingolimod: risk assessment and consensus recommendations for management. *JAMA Neurol.* 72: 31–39.
62. Calvi, A., M. A. Clarke, F. Prados, D. Chard, O. Ciccarelli, M. Alberich, D. Pareto, M. Rodríguez Barranco, J. Sastre-Garriga, C. Tur, et al. 2023. Relationship between paramagnetic rim lesions and slowly expanding lesions in multiple sclerosis. *Mult. Scler.* 29: 352–362.
63. Preziosa, P., E. Pagani, A. Meani, L. Moiola, M. Rodegher, M. Filippi, and M. A. Rocca. 2022. Slowly expanding lesions predict 9-year multiple sclerosis disease progression. *Neurol. Neuroimmunol. Neuroinflamm.* 9: e1139.
64. Elliott, C., D. L. Arnold, H. Chen, C. Ke, L. Zhu, I. Chang, E. Cahir-McFarland, E. Fisher, B. Zhu, S. Gheuens, et al. 2020. Patterning

chronic active demyelination in slowly expanding/evolving white matter MS lesions. *AJNR Am. J. Neuroradiol.* 41: 1584–1591.
65. Steinmaurer, A., C. Riedl, T. König, G. Testa, U. Köck, J. Bauer, H. Lassmann, R. Höftberger, T. Berger, I. Wimmer, et al. 2024. The relation between BTK expression and iron accumulation of myeloid cells in multiple sclerosis. *Brain Pathol.* 34: e13240.
66. The Human Protein Atlas; Single cell types; BTK. Available at: https://www.proteinatlas.org/ENSG00000010671-BTK/single+cell+type. Accessed: September 15, 2024.
67. Rawlings, D. J., A. M. Scharenberg, H. Park, M. I. Wahl, S. Lin, R. M. Kato, A. C. Fluckiger, O. N. Witte, and J. P. Kinet. 1996. Activation of BTK by a phosphorylation mechanism initiated by SRC family kinases. *Science* 271: 822–825.
68. Liu, S., M. Zheng, Y. Li, L. He, and T. Chen. 2020. The protective effect of Geniposide on diabetic cognitive impairment through BTK/TLR4/NF-κB pathway. *Psychopharmacology (Berl)*. 237: 465–477.
69. Chen, T., S. Liu, M. Zheng, Y. Li, and L. He. 2021. The effect of geniposide on chronic unpredictable mild stress-induced depressive mice through BTK/TLR4/NF-κB and BDNF/TrkB signaling pathways. *Phytother. Res.* 35: 932–945.
70. Farahany, J., Y. Tsukasaki, A. Mukhopadhyay, M. Mittal, S. Nepal, C. Tiruppathi, and A. B. Malik. 2022. CD38-mediated inhibition of Bruton's tyrosine kinase in macrophages prevents endotoxemic lung injury. *Am. J. Respir. Cell. Mol. Biol.* 66: 183–195.
71. Owens, T. D., P. F. Smith, A. Redfern, Y. Xing, J. Shu, D. E. Karr, S. Hartmann, M. R. Francesco, C. L. Langrish, P. A. Nunn, et al. 2022. Phase 1 clinical trial evaluating safety, exposure and pharmacodynamics of BTK inhibitor tolebrutinib (PRN2246, SAR442168). *Clin. Transl. Sci.* 15: 442–450.
72. Scheible, H., M. Dyroff, A. Seithel-Keuth, E. Harrison-Moench, N. Mammasse, A. Port, A. Bachmann, J. Dong, J. J. van Lier, W. Tracewell, et al. 2021. Evobrutinib, a covalent Bruton's tyrosine kinase inhibitor: mass balance, elimination route, and metabolism in healthy participants. *Clin. Transl. Sci.* 14: 2420–2430.
73. Ciesielska, A., M. Matyjek, and K. Kwiatkowska. 2021. TLR4 and CD14 trafficking and its influence on LPS-induced pro-inflammatory signaling. *Cell. Mol. Life Sci.* 78: 1233–1261.
74. Ní Gabhann, J., E. Hams, S. Smith, C. Wynne, J. C. Byrne, K. Brennan, S. Spence, A. Kissenpfennig, J. A. Johnston, P. G. Fallon, et al. 2014. Btk regulates macrophage polarization in response to lipopolysaccharide. *PLoS One* 9: e85834.
75. Dobie, G., F. A. Kuriri, M. M. A. Omar, F. Alanazi, A. M. Gazwani, C. P. S. Tang, D. M.-Y. Sze, S. M. Handunnetti, C. Tam, D. E. Jackson, et al. 2019. Ibrutinib, but not zanubrutinib, induces platelet receptor shedding of GPIb-IX-V complex and integrin αIIbβ3 in mice and humans. *Blood Adv.* 3: 4298–4311.
76. Boyle, A. J., A. Lindberg, J. Tong, D. Zhai, F. Liu, and N. Vasdev. 2024. Preliminary PET imaging of [^{11}C]evobrutinib in mouse models of colorectal cancer, SARS-CoV-2, and lung damage: radiosynthesis via base-aided palladium-NiXantphos-mediated ^{11}C-carbonylation. *J. Labelled Comp. Radiopharm.* 67: 235–244.
77. Zhao, M., Y. Wang, L. Li, S. Liu, C. Wang, Y. Yuan, G. Yang, Y. Chen, J. Cheng, Y. Lu, et al. 2021. Mitochondrial ROS promote mitochondrial dysfunction and inflammation in ischemic acute kidney injury by disrupting TFAM-mediated mtDNA maintenance. *Theranostics* 11: 1845–1863.
78. Kumar, P., C. Liu, J. Suliburk, J. W. Hsu, R. Muthupillai, F. Jahoor, C. G. Minard, G. E. Taffet, and R. V. Sekhar. 2023. Supplementing glycine and N-acetylcysteine (GlyNAC) in older adults improves glutathione deficiency, oxidative stress, mitochondrial dysfunction, inflammation, physical function, and aging hallmarks: a randomized clinical trial. *J. Gerontol. A Biol. Sci. Med. Sci.* 78: 75–89.
79. Bharath, L. P., M. Agrawal, G. McCambridge, D. A. Nicholas, H. Hasturk, J. Liu, K. Jiang, R. Liu, Z. Guo, J. Deeney, et al. 2020. Metformin enhances autophagy and normalizes mitochondrial function to alleviate aging-associated inflammation. *Cell. Metab.* 32: 44–55.e6.
80. Domínguez-Mozo, M. I., M. C. García-Frontini Nieto, M. I. Gómez-Calcerrada, S. Pérez-Pérez, M. Á. García-Martínez, L. M. Villar, N. Villarrubia, L. Costa-Frossard, R. Arroyo, R. Alvarez-Lafuente, et al. 2022. Mitochondrial impairments in peripheral blood mononuclear cells of multiple sclerosis patients. *Biology (Basel)* 11: 1633.
81. Sheikh, M. H., S. M. Henson, R. A. Loiola, S. Mercurio, A. Colamatteo, G. T. Maniscalco, V. De Rosa, S. McArthur, and E. Solito. 2020. Immunometabolic impact of the multiple sclerosis patients' sera on endothelial cells of the blood-brain barrier. *J. Neuroinflammation* 17: 153.
82. Europa, T. A., M. Nel, M. R. Lebeko, and J. M. Heckmann. 2022. Mitochondrial bioenergetics in ocular fibroblasts of two myasthenia gravis cases. *IBRO Neurosci. Rep.* 12: 297–302.
83. Qi, H., L. Xu, and Q. Liu. 2023. Knockdown of DEC2 expression inhibits the proliferation of mesangial cells through suppressed glycolysis and p38 MAPK/Erk pathway in lupus nephritis. *Mol. Med.* 29: 99.
84. van Horssen, J., P. van Schaik, and M. Witte. 2019. Inflammation and mitochondrial dysfunction: a vicious circle in neurodegenerative disorders? *Neurosci. Lett.* 710: 132931.
85. Park, M. W., H. W. Cha, J. Kim, J. H. Kim, H. Yang, S. Yoon, N. Boonpraman, S. S. Yi, I. D. Yoo, J.-S. Moon, et al. 2021. NOX4 promotes ferroptosis of astrocytes by oxidative stress-induced lipid peroxidation via the impairment of mitochondrial metabolism in Alzheimer's diseases. *Redox. Biol.* 41: 101947.
86. Das, B., S. P. Dash, S. Mohanty, and P. Patel. 2021. Parkinson's disease and impairment in mitochondrial metabolism: a pathognomic signature. *Adv. Exp. Med. Biol.* 1286: 65–76.
87. Rosenkranz, S. C., A. A. Shaposhnykov, S. Träger, J. B. Engler, M. E. Witte, V. Roth, V. Vieira, N. Paauw, S. Bauer, C. Schwencke-Westphal, et al. 2021. Enhancing mitochondrial activity in neurons protects against neurodegeneration in a mouse model of multiple sclerosis. *Elife* 10: e61798.
88. Plitzko, B., and S. Loesgen. 2018. Measurement of oxygen consumption rate (OCR) and extracellular acidification rate (ECAR) in culture cells for assessment of the energy metabolism. *Bio. Protoc.* 8: e2850.
89. Kelly, B., and L. A. O'Neill. 2015. Metabolic reprogramming in macrophages and dendritic cells in innate immunity. *Cell. Res.* 25: 771–784.
90. Wang, L., S. Pavlou, X. Du, M. Bhuckory, H. Xu, and M. Chen. 2019. Glucose transporter 1 critically controls microglial activation through facilitating glycolysis. *Mol. Neurodegener.* 14: 2.
91. Vaupel, P., and G. Multhoff. 2021. Revisiting the Warburg effect: historical dogma versus current understanding. *J. Physiol.* 599: 1745–1757.
92. Bar-Even, A., A. Flamholz, E. Noor, and R. Milo. 2012. Rethinking glycolysis: on the biochemical logic of metabolic pathways. *Nat. Chem. Biol.* 8: 509–517.
93. Schmidt, C. A., K. H. Fisher-Wellman, and P. D. Neufer. 2021. From OCR and ECAR to energy: perspectives on the design and interpretation of bioenergetics studies. *J. Biol. Chem.* 297: 101140.
94. Qiu, J., Y. Fu, Z. Chen, L. Zhang, L. Li, D. Liang, F. Wei, Z. Wen, Y. Wang, S. Liang, et al. 2021. BTK promotes atherosclerosis by regulating oxidative stress, mitochondrial injury, and ER stress of macrophages. *Oxid. Med. Cell. Longev.* 2021: 9972413.
95. Mukherjee, S., R. N. Ghosh, and F. R. Maxfield. 1997. Endocytosis. *Physiol. Rev.* 77: 759–803.
96. Gensel, J. C., and B. Zhang. 2015. Macrophage activation and its role in repair and pathology after spinal cord injury. *Brain Res.* 1619: 1–11.
97. Milich, L. M., C. B. Ryan, and J. K. Lee. 2019. The origin, fate, and contribution of macrophages to spinal cord injury pathology. *Acta Neuropathol.* 137: 785–797.
98. Sivaraj, K. K., P.-G. Majev, H.-W. Jeong, B. Dharmalingam, D. Zeuschner, S. Schröder, M. G. Bixel, M. Timmen, R. Stange, R. H. Adams, et al. 2022. Mesenchymal stromal cell-derived septoclasts resorb cartilage during developmental ossification and fracture healing. *Nat. Commun.* 13: 571.

99. Zhou, X., S. Wahane, M.-S. Friedl, M. Kluge, C. C. Friedel, K. Avrampou, V. Zachariou, L. Guo, B. Zhang, X. He, et al. 2020. Microglia and macrophages promote corralling, wound compaction and recovery after spinal cord injury via Plexin-B2. *Nat. Neurosci.* 23: 337–350.
100. Martin-Rodriguez, O., T. Gauthier, F. Bonnefoy, M. Couturier, A. Daoui, C. Chagué, S. Valmary-Degano, C. Gay, P. Saas, S. Perruche, et al. 2021. Pro-resolving factors released by macrophages after efferocytosis promote mucosal wound healing in inflammatory bowel disease. *Front. Immunol.* 12: 754475.
101. Amoras, A. L., H. Kanegane, T. Miyawaki, and M. M. Vilela. 2003. Defective Fc-, CR1- and CR3-mediated monocyte phagocytosis and chemotaxis in common variable immunodeficiency and X-linked agammaglobulinemia patients. *J. Investig. Allergol. Clin. Immunol.* 13: 181–188.
102. Cao, X., B. Li, J. Chen, J. Dang, S. Chen, E. G. Gunes, B. Xu, L. Tian, S. Muend, M. Raoof, et al. 2021. Effect of cabazitaxel on macrophages improves CD47-targeted immunotherapy for triple-negative breast cancer. *J. Immunother. Cancer* 9: e002022.
103. Manna, A., S. Aulakh, P. Jani, S. Ahmed, S. Akhtar, M. Coignet, M. Heckman, Z. Meghji, K. Bhatia, A. Sharma, et al. 2019. Targeting CD38 enhances the antileukemic activity of ibrutinib in chronic lymphocytic leukemia. *Clin. Cancer. Res.* 25: 3974–3985.
104. Feng, M., J. Y. Chen, R. Weissman-Tsukamoto, J.-P. Volkmer, P. Y. Ho, K. M. McKenna, S. Cheshier, M. Zhang, N. Guo, P. Gip, et al. 2015. Macrophages eat cancer cells using their own calreticulin as a guide: roles of TLR and Btk. *Proc. Natl Acad. Sci. USA* 112: 2145–2150.
105. Yin, Z., Z. Han, T. Hu, S. Zhang, X. Ge, S. Huang, L. Wang, J. Yu, W. Li, Y. Wang, et al. 2020. Neuron-derived exosomes with high miR-21-5p expression promoted polarization of M1 microglia in culture. *Brain Behav. Immun.* 83: 270–282.
106. Chen, X., X. Wang, Z. Cui, Q. Luo, Z. Jiang, Y. Huang, J. Jiang, J. Qiu, Y. Li, K. Yu, et al. 2023. M1 microglia-derived exosomes promote activation of resting microglia and amplifies proangiogenic effects through Irf1/miR-155-5p/Socs1 axis in the retina. *Int. J. Biol. Sci.* 19: 1791–1812.
107. Xu, Y., C. Zhang, D. Cai, R. Zhu, and Y. Cao. 2023. Exosomal miR-155-5p drives widespread macrophage M1 polarization in hypervirulent *Klebsiella pneumoniae*-induced acute lung injury via the MSK1/p38-MAPK axis. *Cell. Mol. Biol. Lett.* 28: 92.
108. Shi, Y., Z. Li, K. Li, and K. Xu. 2022. miR-155-5p accelerates cerebral ischemia-reperfusion inflammation injury and cell pyroptosis via DUSP14/TXNIP/NLRP3 pathway. *Acta Biochim. Pol.* 69: 787–793.
109. Wen, Q., Y. Wang, Q. Pan, R. Tian, D. Zhang, G. Qin, J. Zhou, and L. Chen. 2021. MicroRNA-155-5p promotes neuroinflammation and central sensitization via inhibiting SIRT1 in a nitroglycerin-induced chronic migraine mouse model. *J. Neuroinflammation* 18: 287.
110. Yang, Z., X. Shi, Z. Gao, and L. Chu. 2022. miR-155-5p in extracellular vesicles derived from choroid plexus epithelial cells promotes autophagy and inflammation to aggravate ischemic brain injury in mice. *Oxid. Med. Cell. Longev.* 2022: 8603427.
111. Galloway, D. A., S. N. Blandford, T. Berry, J. B. Williams, M. Stefanelli, M. Ploughman, and C. S. Moore. 2019. miR-223 promotes regenerative myeloid cell phenotype and function in the demyelinated central nervous system. *Glia* 67: 857–869.
112. Galloway, D. A., S. J. Carew, S. N. Blandford, R. Y. Benoit, N. J. Fudge, T. Berry, G. R. W. Moore, J. Barron, and C. S. Moore. 2022. Investigating the NLRP3 inflammasome and its regulator miR-223-3p in multiple sclerosis and experimental demyelination. *J. Neurochem.* 163: 94–112.